Optimization of dye adsorption capacity and mechanical strength of chitosan aerogels through crosslinking strategy and graphene oxide addition

M. Salzano de Luna[a,b,*], C. Ascione[b], C. Santillo[c], L. Verdolotti[c], M. Lavorgna[c,*], G.G. Buonocore[c], R. Castaldo[b], G. Filippone[a], H. Xia[d], L. Ambrosio[c]

[a] *Department of Chemical, Materials and Production Engineering (INSTM Consortium – UdR Naples), University of Naples Federico II, P.le Tecchio 80, 80125 Naples, Italy*

[b] *Institute for Polymers, Composites and Biomaterials, National Research Council of Italy, Via Campi Flegrei 34, 80078 Pozzuoli, Italy*

[c] *Institute for Polymers, Composites and Biomaterials, National Research Council of Italy, P.le E. Fermi 1, 80055 Portici (Naples), Italy*

[d] *State Key Laboratory of Polymer Materials Engineering, Polymer Research Institute of Sichuan University, Chengdu 610065, China*

Corresponding authors:

[*]e-mail: martina.salzanodeluna@unina.it; phone: +39 0817682407 (Martina Salzano de Luna)

[*]e-mail: mlavorgn@unina.it; phone: +39 0817758838 (Marino Lavorgna)

ABSTRACT

Chitosan (CS) aerogels were prepared by freeze-drying as potential adsorbents for water purification, and the effect of the strategy of crosslinking was investigated by varying the amount of crosslinker (glutaraldehyde) and the sequence of steps for the preparation of the aerogel. Two procedures were compared, in which the crosslinking step was carried out before or after the freeze-drying of the starting CS solution. When crosslinking was postponed after the freeze-drying step, the adsorption capacity towards an anionic dye, such as indigo carmine, considerably increased (up to +45%), reaching values as high as 534.4 ± 30.5 mg g^{-1}. The same crosslinking strategy ensured a comparable improvement also in nanocomposite aerogels containing graphene oxide (GO), which was added to enhance the mechanical strength and provide adsorption capacity towards cationic dyes. Besides possessing good mechanical strength (compressive modulus higher than 1 MPa), the CS/GO aerogels were able to bind also cationic pollutants such as methylene blue. The maximum uptake capacity increased from 4.3 ± 1.6 to 168.6 ± 9.6 mg of cationic dye adsorbed per gram of adsorbent with respect to pristine CS aerogels.

GRAPHICAL ABSTRACT

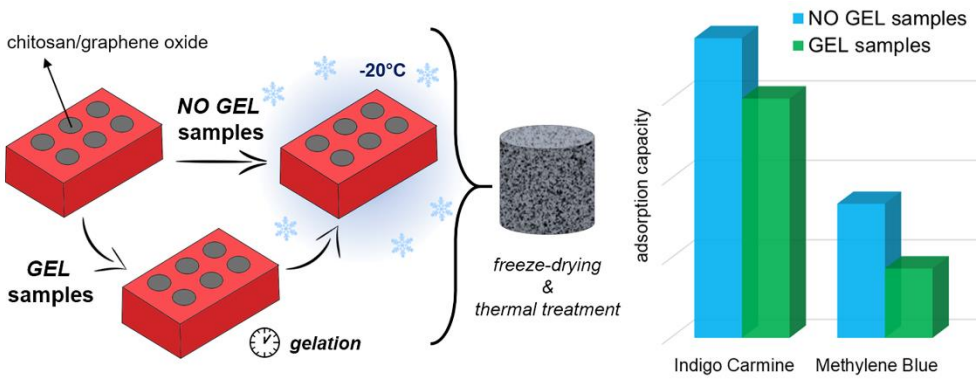

KEYWORDS. chitosan; aerogel; graphene oxide; crosslinking; mechanical properties; dye removal

1. INTRODUCTION

Aerogels are a fascinating class of highly porous materials widely used in a number of applications in which high pore volume and large surface area play major roles (Smirnova & Gurikov, 2017; Zhao et al., 2018). Originally employed mostly for thermal insulation purposes, in recent years aerogels are finding many new fields of application, ranging from life science (Maleki et al., 2016) to food (Mikkonen, Parikka, Ghafar, & Tenkanen, 2013) and catalysis (Wan, Zhang, Ma, & Zhou, 2018). One of the main sectors in which aerogels are being successfully employed is the environmental one (Maleki, 2016). In the specific field of water remediation, biopolymer-based aerogels, and in particular chitosan (CS)-based ones, are receiving growing attention (Bhatnagar & Sillanpää, 2009; Vakili et al., 2014; Olivera et al., 2016). CS possesses amine and hydroxyl groups, which are highly effective in binding both anionic pollutants and heavy metal ions (Crini, & Badot, 2008). Apart from the chemical features, the adsorption capacity of CS-based aerogels can be optimized by controlling their porosity and surface area. Being the latter strictly related to the conditions of preparation, the optimization of the production process represents a crucial aspect for the maximization of the performances of CS adsorbent for wastewater treatment (Salzano de Luna et al., 2017a).

Among the possible ways of producing CS aerogels, the freeze-drying of CS hydrogels is one of the most effective (Quignard, Valentin, & Di Renzo, 2008). The challenge is obtaining a material that is highly porous, but also mechanically stable in order to be handled and possibly

regenerated and reused. The polymer concentration in the starting solution is the main parameter on which researchers have focused their attention aiming at identifying the proper trade-off between adsorption capacity and mechanical strength. As an example, Wang et al. recently showed that freeze-casted CS sponges realized from solutions at low polymer concentration have the highest adsorption capacity towards Rose Bengal dye (Wang *et al.*, 2017). However, a compromise has to be sought for avoiding the collapse of the starting hydrogel, which must contain enough polymer for retaining its shape and size both in the swollen state and during the sublimation step. A possible strategy for enhancing the mechanical stability of aerogels is the addition of reinforcing (nano)fillers. Among others, graphene oxide (GO) has been lately used due to its tendency to self-assemble with CS chains in acid solution, thus contributing in stabilizing the hydrogel before the freeze-drying step (Zhang et al., 2011; Chen, Chen, Bai, & Li, 2013). The use of GO brings about the additional advantage of an improved adsorption capacity, which is due to its inherent affinity towards specific classes of water pollutants (Kemp et al., 2013; Chabot et al., 2014). Unfortunately, CS/GO aerogels are relatively unstable and tend to dissolve even in weakly acid conditions (Frindy et al., 2017). To overcome this issue, robust CS-based hydrogels can be obtained by using two different approaches, namely the physical or chemical crosslinking processes (Berger et al., 2004; Bhattarai, Gunn & Zhang, 2010). In the present work, the attention is focused on the latter strategy, and particularly on the use of small bi-functional molecules as chemical crosslinking agents. Among them, dialdehydes have been often investigated and their effectiveness has been widely proven (Chang, Chen, & Jiao, 2008; Yu et al., 2017; Omidi & Kakanejadifard, 2018). However, the crosslinking reaction involves functional groups of the CS chain, thus reducing the number of active sites in the adsorption process (Zhang et al., 2011). For this reason, the amount of crosslinker has to be contained as

much as possible (Li et al., 2016); nonetheless, its use is essential for preserving mechanical and chemical stability of CS-based aerogels obtained through freeze-drying. Despite its importance, in the literature there is a surprising lack concerning the crosslinking strategies, which are systematically relegated to the secondary role of intermediate step to be performed *before* freezing the resulting hydrogel. In this work we show for the first time that the crosslinking step is actually a key-parameter for optimizing the adsorption performance of CS aerogels. In particular, simply postponing the crosslinking step *after* freeze-drying results in a considerable increase in the adsorption capacity of CS aerogels without significant losses in terms of mechanical properties. The latter can be anyhow enhanced through the addition of GO. Besides possessing improved mechanical strength, the nanocomposite CS/GO aerogels also exhibit broad-spectrum adsorption capacity, being able to remove both anionic and cationic pollutants from water.

2. EXPERIMENTAL SECTION

2.1. Materials

Medium molecular weight chitosan powder was purchased from Sigma Aldrich. Its deacetylation degree was determined to be ~77% through the FTIR method proposed by Sabnis and Block (Sabnis & Block, 1997). Graphite flakes (Qingdao Dahe Graphite Co. Ltd, China) were used for the preparation of graphene oxide nanosheets through the Hummers method (Hummers & Offeman, 1958). Glutaraldehyde (GA) aqueous solution (25 wt.%), Indigo Carmine (IC), and Methylene Blue (MB) were purchased from Sigma Aldrich.

2.2. Aerogel preparation

CS powder (20 mg mL^{-1}) was dissolved in 0.35 M acetic acid solution at room temperature, and then GA aqueous solution was added under stirring. The GA concentration, Φ_{GA}, was varied from 5 to 15 wt.% with respect to the CS amount. The CS/GA solutions were rapidly poured into PDMS stamps. Two sets of samples were prepared through the distinct procedures sketched in Figure 1.

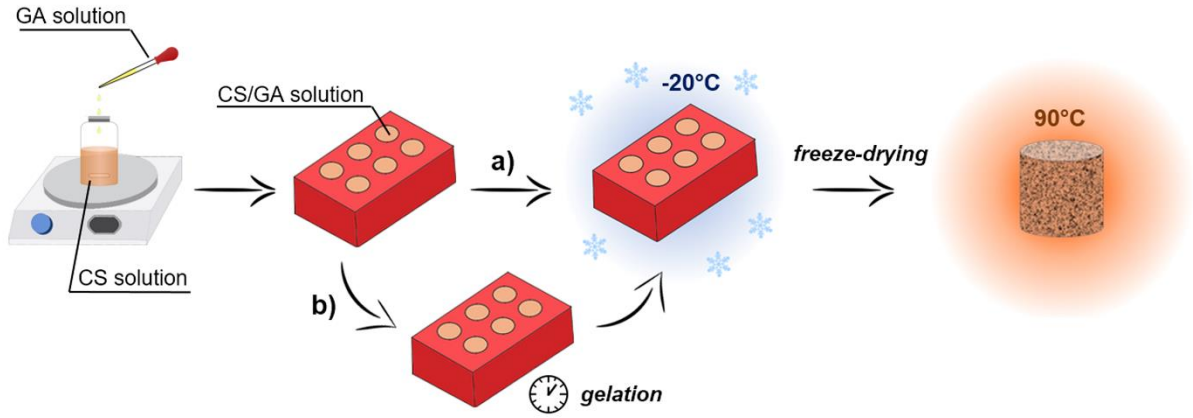

Figure 1. Schematic representation of the crosslinking strategies adopted for the realization of a) no-GEL and b) GEL aerogels.

In one case, the samples, hereinafter named as "no-GEL", were immediately frozen in a refrigerator at -20°C. A second set of samples, below referred to as "GEL", was instead allowed to gel at room temperature for 24 hours, and then was frozen at -20°C. The incipient crosslinking occurring in the no-GEL samples before and during the freezing step is definitely negligible with respect to the case of the GEL samples (Supplementary Material, Section S1). After being completely frozen, both the no-GEL and GEL samples were lyophilized in a vacuum freeze-dryer. Finally, the as-obtained CS aerogels were subjected to a mild thermal treatment (90°C, 1 hour). This last step was carried out to allow the completion of crosslinking reaction between CS

and GA in the no-GEL samples (Yu et al., 2017). The GEL samples, for which the crosslinking already took place before the freezing step, were subjected to the same thermal treatment for the sake of comparison. Note that the conditions of the thermal treatment were sufficient for the completing of the crosslinking reactions (Supplementary Material, Section S2).

For the preparation of nanocomposite aerogels, GO (10 mg mL^{-1}) was dispersed in bi-distilled water by ultrasonication. Acetic acid was added to get a 0.35 M solution. Afterwards, CS powder (20 mg mL^{-1}) was slowly added to the GO dispersion under magnetic stirring at room temperature until complete dissolution. The CS/GO weight ratio was fixed to 2/1. After addition of GA (Φ_{GA} = 10 wt.% with respect to the amount of CS and GO), the realization of no-GEL and GEL CS/GO aerogels was carried out following the same procedures previously described for pristine CS aerogels.

2.3. Characterization

Rheological measurements were performed by means of a stress-controlled rotational rheometer (ARG2, TA Instruments) in cone-plate geometry (diameter 40 mm, angle 2°) with a Peltier base for temperature control. Time sweep experiments were performed to study the crosslinking kinetics at different Φ_{GA}. The storage, G', and loss, G'', moduli were monitored over time at 1 rad s^{-1} and temperature T = 25°C. Frequency sweep tests were carried out on CS hydrogels crosslinked with different amounts of glutaraldehyde, Φ_{GA}. The experiments were performed on samples after 24 hours that GA was added to the CS solution. The viscoelastic moduli were monitored in the linear regime in the frequency range ω = 0.1-100 rad s^{-1}.

Fourier Transform Infrared (FTIR) spectroscopy was carried out in Attenuated Total Reflectance (ATR) mode with a Perkin Elmer Spectrum One spectrometer. The ATR spectra were recorded

151 at a resolution of 4 cm^{-1} and 64 scan collections. Baseline correction was applied to the reported
152 spectra.
153 Scanning electron microscopy (SEM) analyses were carried out using a FEI Quanta 200 FEG
154 microscope in high vacuum mode. The observations were performed on aerogels previously cut
155 with a razor blade and sputter coated with a 15 nm thick Au-Pd layer.
156 The apparent density of the aerogels, ρ_A, was calculated as:

157 $$\rho_A = \frac{m}{\pi \left(D/2\right)^2 H} \quad (1)$$

158 where m is the mass of aerogel, and D and H represent the diameter and the height of the sample,
159 respectively.
160 The percentage porosity of the aerogels was estimated from both apparent density data (P_D) and
161 liquid infusion measurements (P_L). In detail, P_D, was calculated as:

162 $$P_D = \left(1 - \frac{\rho_A}{\rho_S}\right) \cdot 100\% \quad (2)$$

163 where ρ_S is the skeletal density of the aerogel measured by helium pycnometer (Supplementary
164 Material, Section S3). P_L was instead measured by immersing weighed dry aerogels in an excess
165 volume of ethanol, which was forced to enter the accessible pores through vacuum cycles.
166 Absolute ethanol was used as testing liquid because it is a non-solvent but easily penetrates into
167 the pores without inducing shrinkage or swelling (Nieto-Suárez, López-Quintela, & Lazzari,
168 2016). Equilibrium was considered attained when the weight of the aerogels after immersion was
169 found to be constant over time. P_L was calculated using the following formula (Tan, Wu, Lao, &
170 Gao, 2009):

171 $$P_L = \left(\frac{m_{EtOH}/\rho_{EtOH}}{\pi \left(D/2\right)^2 H}\right) \cdot 100\% \quad (3)$$

where ρ_{EtOH} is the ethanol density and m_{EtOH} represents the mass of liquid penetrated in the aerogel porosity at equilibrium, which has been calculated as weight difference of the samples before and after immersion in ethanol.

Mechanical tests were performed on cylindrical aerogels (area A_0, height h_0) by compression tests. The samples were subjected to 100 squeezing cycles up to 25% of deformation at 5 μm s^{-1}. The normal force, F_N, and plate displacement, Δh, were recorded over time, and the engineering stress, σ, and strain, ε, were calculated as:

$$\sigma = \frac{F_N}{A_0} \quad (4)$$

$$\varepsilon = \frac{\Delta h}{h_0} \quad (5)$$

The compressive modulus, E_c, was estimated in the linear region of the σ-ε curves, and the residual deformation after each loading-unloading cycle, ε_R, was recorded.

The dye adsorption behavior was investigated by batch tests. The aerogels were weighed and put in propylene tubes containing dye solutions at different concentration. The experiments were performed at neutral pH conditions. The tubes were agitated at 200 rpm at constant temperature (T = 27°C) by using a thermostated shaker with controlled temperature (SKI 4, Argo Lab). The equilibrium dye concentration after the adsorption process was determined by analyzing the solutions with a spectrophotometer at the characteristic maximum absorbance wavelength of each of the used dyes (611 nm for IC and 665 nm for MB). The equilibrium adsorption capacity, q_e, was determined as:

$$q_e = \frac{V\left(C_0 - C_e\right)}{m} \quad (6)$$

where C_0 is the initial dye concentration, C_e is the equilibrium dye concentration, m is the mass of dry aerogel, and V is the volume of dye solution.

3. RESULTS AND DISCUSSION

3.1. Kinetics and mechanism of crosslinking reaction

For a clear discrimination between samples subjected to crosslinking before and after the freeze-drying step, the time window available before gelation has to be determined for the preparation of the no-GEL samples. At the same time, the samples classified as GEL have to be obtained starting from fully crosslinked hydrogels. Both these aspects were assessed through rheological analyses. The chemical gelation of chitosan with GA depends on various parameters, such as pH, ionic strength, temperature, CS and GA concentration (Roberts & Taylor, 1989; Argüelles-Monal, Goycoolea, Peniche, & Higuera-Ciapara, 1998). For our purposes, only Φ_{GA} was varied while keeping fixed all other variables. As soon as GA is added, the CS solutions exhibited a typical liquid-like behavior ($G'' > G'$) irrespective of the GA concentration (inset of Figure 2a). Both moduli increase over time, the growth of G' being more pronounced. As a result, G' reaches and eventually surpasses G'' at a certain time instant, t_{GEL}, which can be taken as a rough – and yet sufficient for our purposes – estimate of the "gel time" (Normand, Muller, Ravey, & Parker, 2000). The so-obtained values of t_{GEL} are reported in Figure 2a as a function of the amount of crosslinker.

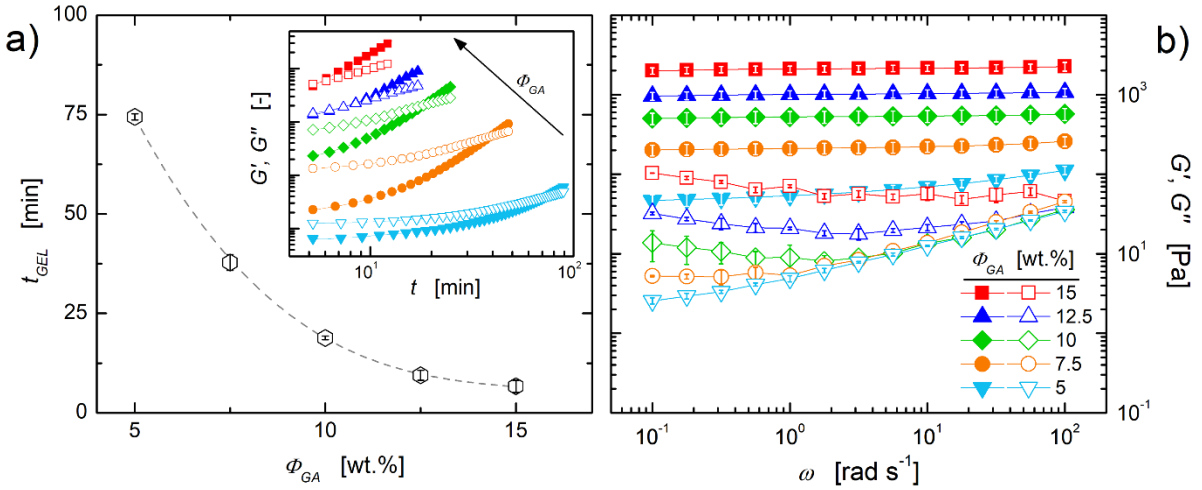

Figure 2. a) Gel time of CS solutions at different Φ_{GA}. Representative time-dependent storage (full symbols) and loss (empty symbols) moduli are reported in the inset. The curves have been vertically-shifted for the sake of clarity, from bottom to top: Φ_{GA} = 5, 7.5, 10, 12.5, and 15 wt.%. b) Frequency-dependent storage (full symbols) and loss (empty symbols) modulus for CS hydrogels crosslinked with different Φ_{GA}; the curves refer to samples 24 hours after GA addition to the CS solution. The error bars represent the standard deviation over three independent measurements.

As expected, the more GA is added to the CS solution, the shorter is t_{GEL} (Roberts & Taylor, 1989; Mi et al., 2000). Stable hydrogels were not obtained at Φ_{GA} = 2.5 wt.%, at least in the adopted processing conditions (Supplementary Material, Section S4). On the other hand, samples at Φ_{GA} > 15 wt.% were not considered as the rapidity of the gelation makes it difficult to obtain a truly no-GEL sample. Frequency sweep tests confirmed that all the samples prepared according the GEL procedure were fully crosslinked before freeze-drying, as proved by the frequency independence of G' (Figure 2b).

FTIR analyses was performed on no-GEL and GEL aerogels at the end of the thermal treatment to investigate possible effects of the different crosslinking strategy on the reaction path. The results are shown in Figure 3 for two samples at low (5 wt.%) and high (15 wt.%) GA content.

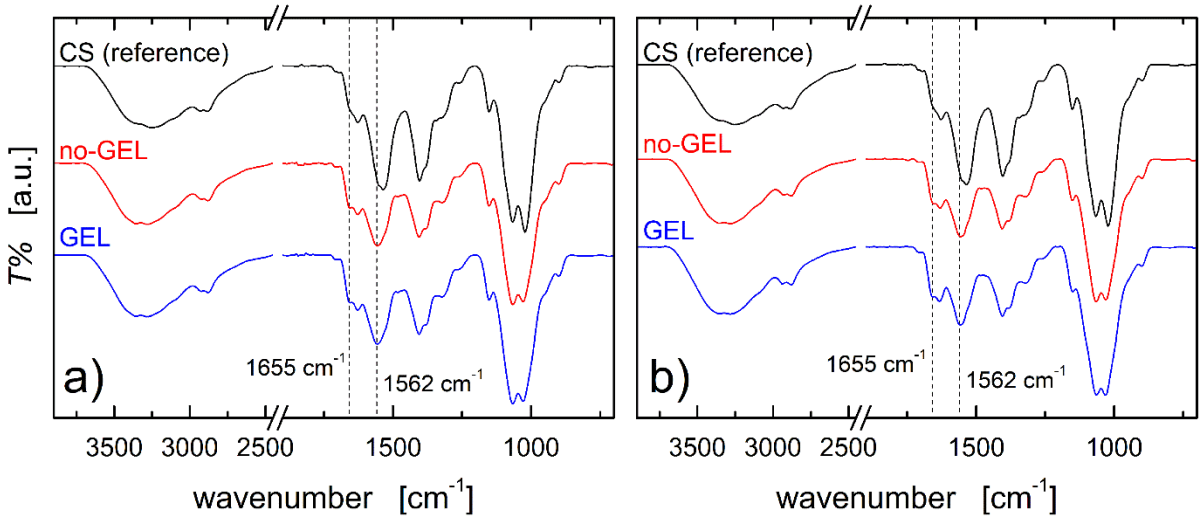

Figure 3. FTIR spectra of no-GEL and GEL CS aerogels crosslinked with Φ_{GA} = a) 5 and b) 15 wt.% after thermal treatment. The spectrum of not crosslinked CS aerogel is also reported as reference.

In the spectrum of not crosslinked CS aerogel, the typical stretching vibrations of hydroxyl and ammine groups can be observed around 3300 cm^{-1}. In addition, CH_3 symmetric stretching, C–O–C stretching, and C–OH stretching can be recognized at around 2936 cm^{-1}, 1150 cm^{-1} and 1065 cm^{-1}, respectively (Lavorgna, Piscitelli, Mangiacapra, & Buonocore, 2010; Nagireddi, Katiyar, & Uppaluri, 2017). In the spectra of crosslinked CS aerogels, the appearance of a peak at 1655 cm^{-1} and a shoulder at 1562 cm^{-1} can be attributed to the formation of imine N=C and ethylenic C=C bonds, respectively. These new vibration bands indicate that a Schiff base reaction occurred between CS chains and GA molecules, and this holds true regardless of the concentration of GA

used and the procedure adopted for the preparation of aerogels. Furthermore, the absence of the peak at 1720 cm^{-1} related to free aldehydic groups indicates that unreacted GA is not detectable in the aerogels (Monteiro & Airoldi, 1999). The results of FTIR are in agreement with gel fraction measurements (Supplementary Material, Section S5), which confirm the occurrence of the crosslinking reactions irrespective of preparation procedure and amount of GA.

3.2. Effect of crosslinking strategy on the structure and properties of the CS aerogels

The morphology of no-GEL and GEL CS aerogels is shown in Figure 4 for representative samples prepared with low (5 wt.%) and high (15 wt.%) GA content.

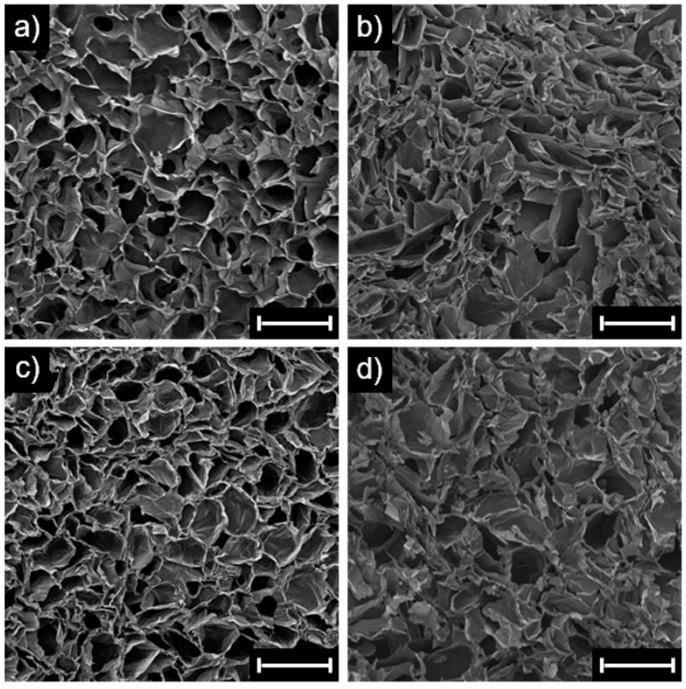

Figure 4. SEM micrographs of cross-sectioned a, b) no-GEL and c, d) GEL CS aerogels crosslinked with Φ_{GA} = a, c) 5 wt.% and b, d) 15 wt.%. The scale bars correspond to 500 µm.

The aerogels at low Φ_{GA} (Figure 4a and c) are characterized by a cellular structure, with pore size ranging from several tens to few hundreds of microns. The no-GEL sample exhibits a more homogeneous pore size distribution, whereas non-spherical and elongated pores with crumpled and thicker cell walls are noticed in the GEL sample. At high Φ_{GA} (Figure 4b and d), the porous structure of the aerogels becomes less regular, and no clear differences can be noticed between the no-GEL and GEL samples. Actually, despite the apparent morphological similarity on the scale of hundreds of microns, the data of apparent density and porosity reveal the existence of subtle differences between the two sets of samples (Figure 5).

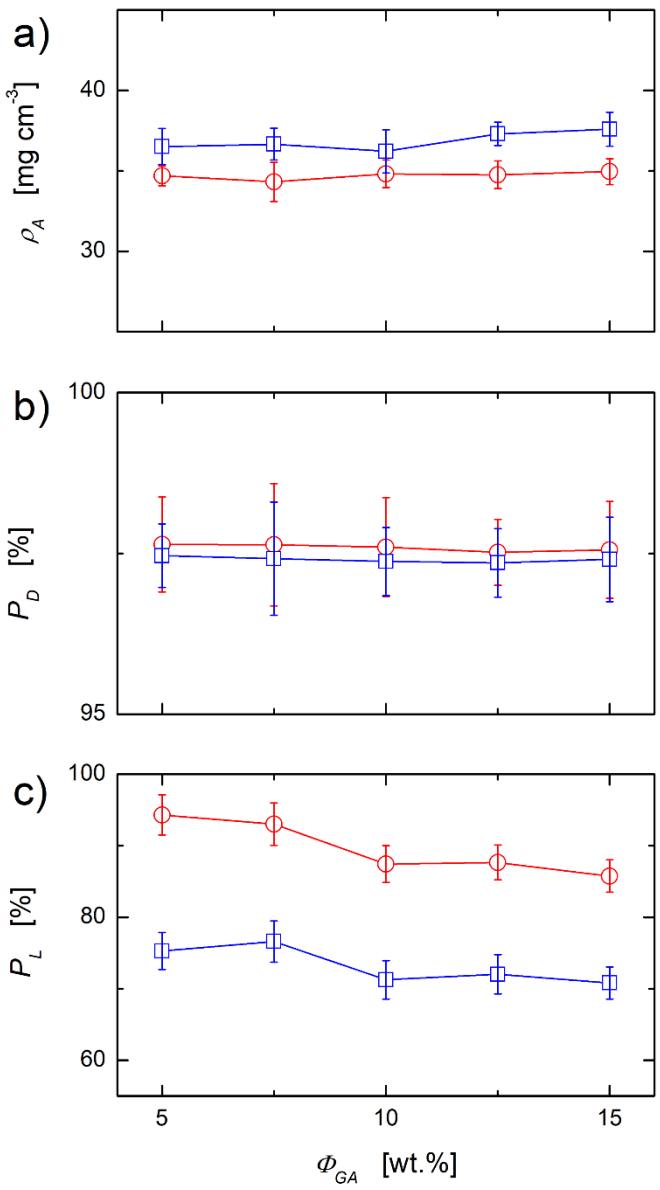

Figure 5. a) Apparent density, b) percentage porosity calculated from density data, and c) percentage porosity obtained from liquid infusion measurements for no-GEL (red circles) and GEL (blue squares) CS aerogels crosslinked with different Φ_{GA}. The error bars represent the standard deviation over ten independent measurements.

The apparent density of the no-GEL CS aerogels (~35 mg cm^{-3}) is slightly lower than that of GEL ones (~37 mg cm^{-3}). Both values are in line with recent literature data on similar systems

(Wang et al., 2017). Moreover, ρ_A is almost independent from Φ_{GA} in both systems, in agreement with results by Ye et al. on poly(vinyl alcohol)/GO aerogels crosslinked (before freeze-drying) with different contents of glutaraldehyde (Ye, Liu, & Feng, 2017). Since the values of ρ_A are comparable for no-GEL and GEL systems, the aerogel porosity determined from density data (P_D) is essentially the same irrespective of the crosslinking strategy (Figure 5b). On the other hand, a significant difference is found between the two sets of samples when the aerogel porosity is measured by liquid infusion method (Figure 5c). The no-GEL samples exhibit much higher P_L values than the GEL ones. Moreover, a slight inverse dependence of P_L on the amount of crosslinker can be noticed. Although the comparable values of ρ_A indicate that the total volume of voids is the same, this result points out that the degree of interconnectivity of the porosity is different in the two systems. For no-GEL aerogels P_L was found to be very similar to P_D, meaning that the porosity of this sample is fully interconnected. This is likely due to the untimely freezing of these samples, which preserves the fine aerogel texture against collapse driven by capillary tension (Valentin et al., 2005). In contrast, a partial loss of pore interconnectivity occurs in the GEL samples, which are left for 24 hours at room temperature for the completing of the crosslinking step. As a result, in the GEL samples P_L is much lower than P_D, being about 20% lower than the P_D of the no-GEL systems.

Another important difference between the no-GEL and GEL aerogels is related to their swelling properties (Supplementary Material, Section S6). In both sets of samples, the swelling degree, *SD*, monotonically decreases upon increasing the amount of GA. This is due to the increasingly higher hydrophobic character of GA-crosslinked chitosan (Poon, Wilson, Headley, 2014) and to the higher rigidity of the CS aerogels in the presence of a higher number of chemical crosslinks, which limit the deformability of the polymer network. It is worth noting that the swelling degree

of the no-GEL samples is systematically higher than that of GEL ones. This result can be correlated to both the different microstructure of the two sets of samples and to a higher rigidity of the CS architecture, which is thus less prone to swell in the presence of water.

The observed differences in the microstructural features of the CS aerogels produced with the two different crosslinking strategies have a strong impact on the macroscopic performances. The mechanical properties of the aerogels were investigated through cyclic compression tests. The results are reported for two representative samples, namely no-GEL and GEL aerogels at Φ_{GA} = 5 wt.%, in Figure 6a and 6b, respectively.

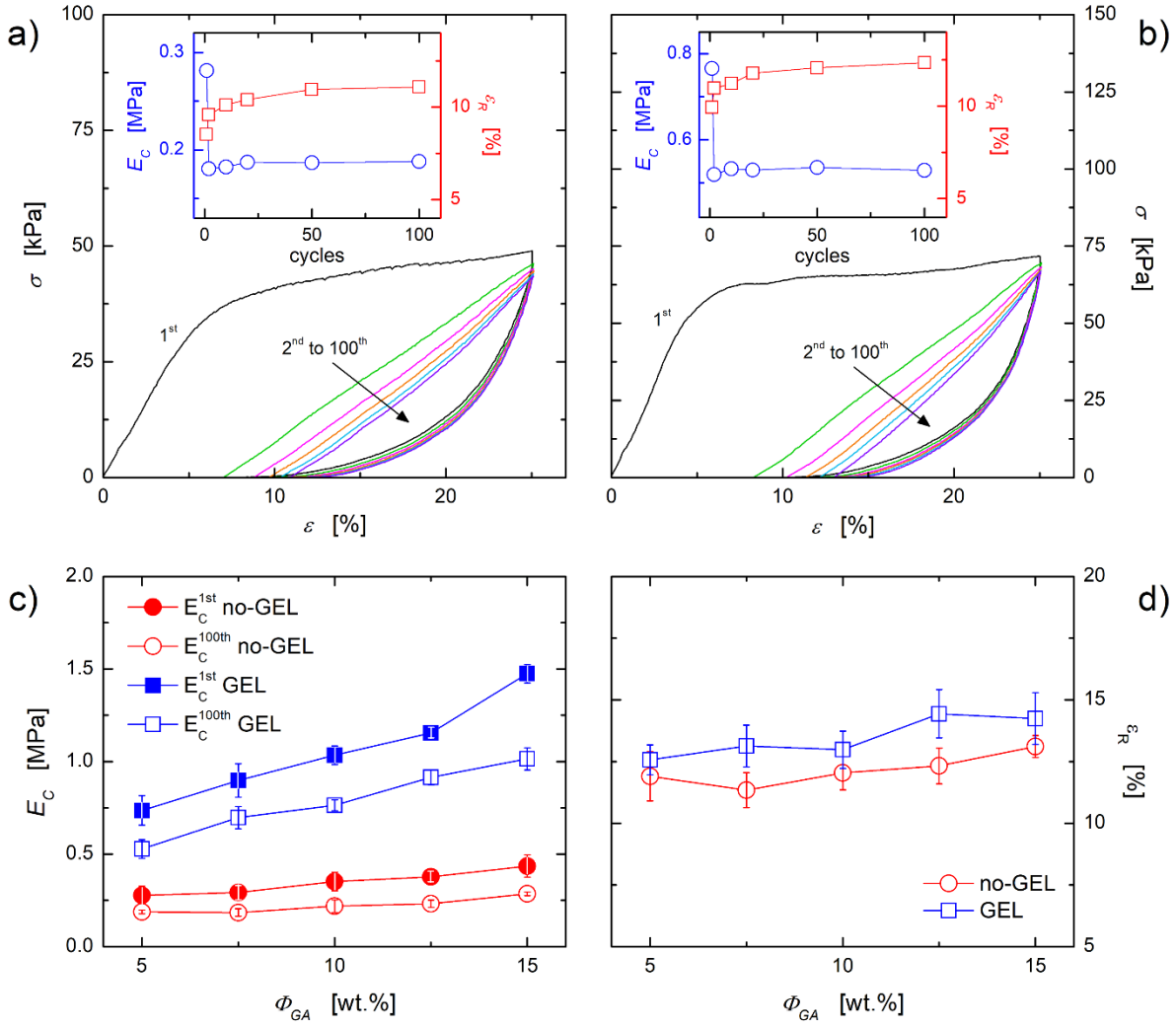

Figure 6. Representative stress-strain curves of a) no-GEL and b) GEL CS aerogels at Φ_{GA} = 5 wt.%. The compressive modulus and residual deformation over different loading/unloading cycles are reported in the insets. c) Compressive modulus calculated at the first and last loading cycle and d) residual deformation (100th cycle) as a function of Φ_{GA} for no-GEL and GEL CS aerogels. The error bars represent the standard deviation over five independent measurements.

The σ-ε curves are characterized by an elastic region (ε < 5%), corresponding to the bending of cell walls, followed by a plateau region due to buckling phenomena (Ye, Liu, & Feng, 2017). For both the no-GEL and GEL systems, E_C is almost halved after the first loading-unloading cycle

due to permanent cracking of the aerogel structure upon compression. The subsequent compression cycles do not cause further decrease of E_c (insets of Figure 6a and 6b). A similar trend was observed for ε_R, which gradually increases until reaching a constant value. The aerogels at higher Φ_{GA} share the same qualitative behavior. For both sets of samples, increasing Φ_{GA} causes an improvement of the mechanical strength, which is in line with previously reported results (Li et al., 2016). In particular, both the compressive modulus of the first (E_C^{1st}) and last (E_C^{100th}) cycle monotonically increase with the crosslinker content (Figure 6c), while Φ_{GA} has a negligible effect on the residual deformation (Figure 6d). Regarding the effect of the crosslinking strategy, the E_C of the GEL samples is about twice that of the no-GEL ones, whereas the values of ε_R are only slightly affected. It is interesting to observe that the subtle morphological differences emerged from the analysis of apparent density and porosity data end up having a substantial effect on the compressive modulus. However, it should be noted that the no-GEL samples keep a sufficiently high compressive modulus, ranging from 0.28 ± 0.05 MPa to 0.44 ± 0.06 MPa at Φ_{GA} = 5 and 15%, respectively.

Due to its inherent affinity with CS-based adsorbents, Indigo Carmine was selected as probing anionic pollutant for investigating the adsorption behavior of the CS aerogels obtained with the different crosslinking strategies. The results of the adsorption tests are shown in Figure 7, where the equilibrium adsorption capacity is reported for the no-GEL and GEL samples as a function of the equilibrium dye concentration.

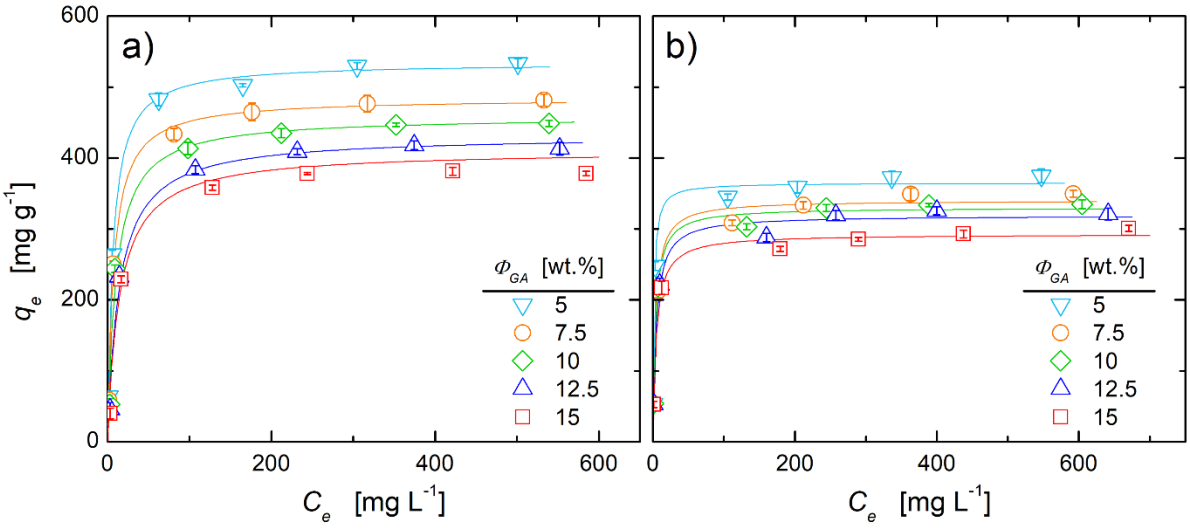

Figure 7. Equilibrium adsorption isotherms for a) no-GEL and b) GEL CS aerogels crosslinked with different Φ_{GA} in the presence of IC. Solid lines correspond to the best fitting with the Langmuir isotherm model. The error bars represent the standard deviation over three independent measurements.

The adsorption isotherms of both no-GEL and GEL CS aerogels share the same qualitative trend: q_e rapidly increases at low dye concentrations, and then it reaches a plateau that is distinctive of an equilibrium saturation point. Such a behavior is typical of homogeneous adsorption processes, in which all the adsorption sites share the same affinity for the adsorbate. In similar cases, the Langmuir isotherm model (Langmuir, 1916) is more suitable than the Freundlich one (Freundlich, 1906) to describe the adsorption behavior (Supplementary Material, Section S7). Apart from the similarity in the overall trend, Figure 7 clearly shows that the adsorption capacity of the no-GEL CS aerogels is significantly higher than that of GEL systems for each investigated value of Φ_{GA}. The observed increase ranges between 35% and 45%, which is higher than the percentage difference between no-GEL and GEL samples in terms of interconnected porosity P_L (see Figure 5.c). This suggests that the better performances of the no-GEL samples could not be

356 solely due to a difference in terms of accessible porosity, but additional mechanisms can also
357 play a role. Although the dye removal process is essentially governed by adsorption phenomena
358 (Supplementary Material, Section S8), the differences in the swelling behavior also play a role in
359 determining the overall dye uptake capacity of the aerogels. Indeed, the interactions among dye
360 molecules and active sites for adsorption in the internal pore surface of the aerogels are expected
361 to be favored in the case of a high *SD* value. The data of Figure 7 also show that the dye uptake
362 capacity steadily diminishes when increasing the amount of crosslinker for both no-GEL and
363 GEL aerogels. This is due to the decrease of available active sites for adsorption due the
364 crosslinking reaction between amine groups of CS chains and GA molecules (see Figure 3).
365
366
367 *3.3. Effect of crosslinking strategy on the properties of nanocomposite CS/GO aerogels*
368 The addition of nanoparticles is often proposed as a powerful strategy for improving the
369 performances of CS-based adsorbents and/or imparting them new functionalities (Chen, Chen,
370 Bai, & Li, 2013; Salzano de Luna et al., 2017b). Zhang et al. already showed that the addition of
371 GO has a beneficial effect on the mechanical properties of not crosslinked CS aerogels (Zhang et
372 al., 2011). However, the way in which the crosslinking strategy may affect the properties of
373 nanocomposite aerogels remains poorly understood. CS/GO systems were realized following the
374 two preparation procedures previously described for pristine CS aerogels. Note that, since the
375 presence of GO nanosheets has a negligible effect on the gelation kinetics of the CS solution
376 (Supplementary Material, Section S9), the distinction between no-GEL and GEL samples
377 remains meaningful.

The mechanical performances of CS/GO aerogels obtaining through the two different crosslinking strategies (Φ_{GA} = 10 wt.%) are summarized in Figure 8. The compressive modulus is calculated at the first cycle, whereas the residual deformation refers to the 100th cycle.

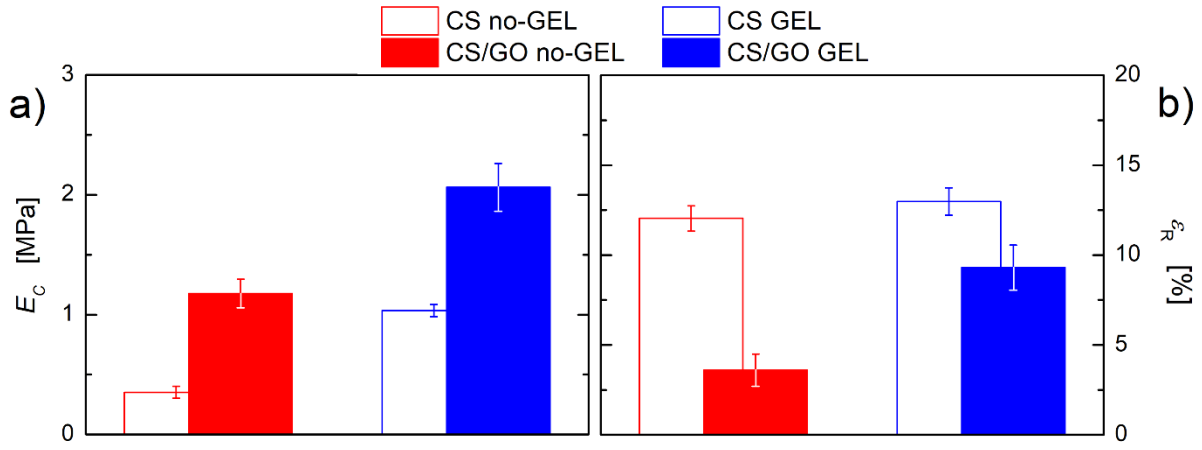

Figure 8. a) Compressive modulus (1st cycle) and b) residual deformation after 100 cycles for no-GEL and GEL CS/GO nanocomposite aerogels. Φ_{GA} was 10 wt.%. The data of pristine CS aerogels are also reported as reference. The error bars represent the standard deviation over five independent measurements.

The compressive modulus of the CS/GO aerogels is significantly improved with respect to pristine systems, and this holds true for both the classes of samples. This means that the crosslinking strategy is an important parameter to act on, even in case of nanocomposite CS aerogels. The effect is much more pronounced for the no-GEL sample, whose modulus increases by about 200%. The toughness also benefits from addition of GO nanosheets, with a significant reduction of the extent of plastic deformation after 100 loading/unloading cycles. The no-GEL system exhibits a better recoverability, with a decrease of the residual deformation of about 70%. Overall, these results prove that the addition of GO mitigates the detrimental effect of the no-

GEL crosslinking strategy, which should be definitely preferred if the goal is achieving high adsorption capacity. The latter also benefits from the inherent adsorption capacity of the GO. Chitosan-based adsorbents are indeed well-known for their outstanding ability in trapping anionic pollutants, while their effectiveness towards cationic dyes is rather scarce because of adverse electrostatic interactions (Crini, & Badot, 2008). On the contrary, thanks to its peculiar surface chemistry, GO is particularly suitable for the removal of positively charged molecules (Chen, Chen, Bai, & Li, 2013). For this reason, the adsorption capacity of no-GEL and GEL CS/GO nanocomposite aerogels was tested using Methylene Blue as cationic dye probe. The equilibrium adsorption capacity of the sample at Φ_{GA} = 10 wt.% is reported in Figure 9 as a function of the equilibrium dye concentration for no-GEL and GEL CS/GO aerogels.

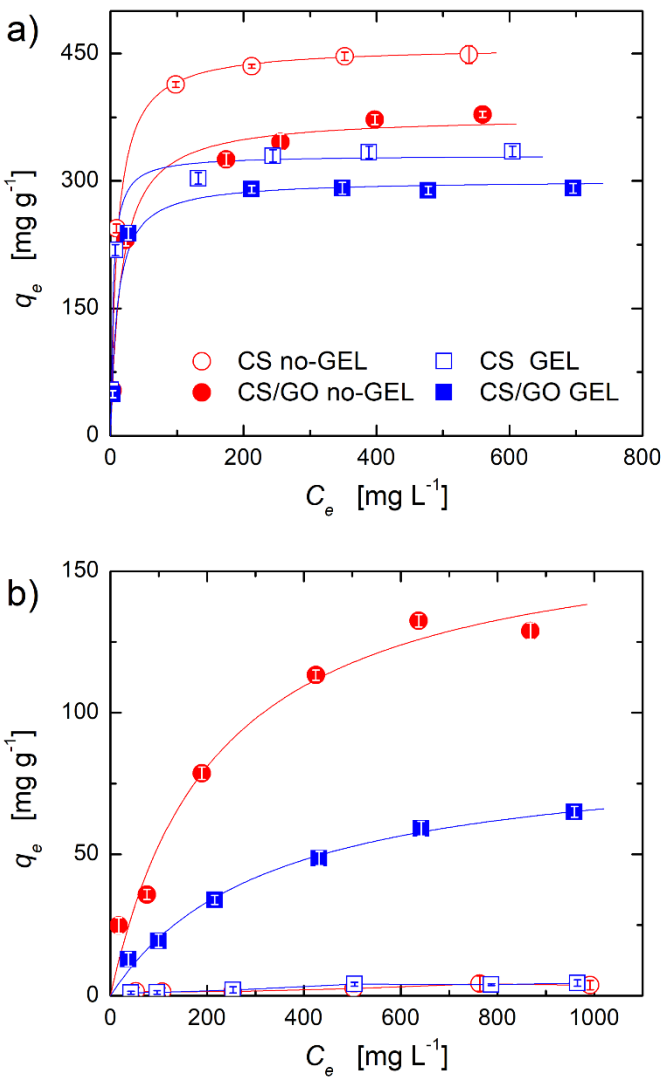

406

407 **Figure 9.** Equilibrium adsorption isotherms for no-GEL (blue squares) and GEL (red circles)
408 CS/GO aerogels (Φ_{GA} = 10 wt.% with respect to the amount of CS and GO) in the presence of a)
409 IC and b) MB. Sample legend is reported in part a). Solid lines correspond to the best fitting with
410 the Langmuir isotherm model. The error bars represent the standard deviation over three
411 independent measurements.

412

413 The Langmuir model well fits the adsorption isotherms of all the investigated samples in the case
414 of both anionic and cationic pollutants (Supplementary Material, Section S10). This suggests that

the presence of GO does not significantly alter the adsorption mechanism of the developed aerogels significantly. The adsorption ability towards IC of the CS/GO aerogels is slightly reduced with respect to pristine CS one, due to the low affinity between GO and IC molecules. Moreover, part of the amino groups of the CS chain, which are active sites for IC adsorption, interacts with the functionalities of the GO nanosheets. On the other hand, this slight decrease (about 10%) is largely offset by the acquisition of appreciable adsorption capacity towards MB. In particular, the maximum adsorption capacity inferable from fitting the experimental data with the Langmuir model grows up to 168.6 ± 9.6 and 87.2 ± 5.2 mg g^{-1} for the no-GEL and GEL sample, respectively (Supplementary Material, Section S10). Overall, our results in terms of mechanical strength and broad-spectrum adsorption capacity (i.e. removal ability towards both anionic and cationic dyes) proved that postponing the crosslinking after the freeze-drying step is extremely preferable for the development of highly performing adsorbents for water purification. This is also highlighted in Table 1, in which the properties of the no-GEL CS/GO aerogel are compare to those of comparable systems reported in the literature.

Table 1. Comparison of the maximum dye adsorption capacity and mechanical performances of the CS/GO aerogel obtained performing the crosslinking after the freeze-drying (no-GEL sample) with literature data on comparable systems.

	Adsorbent	Max q_e for IC [mg g^{-1}]	Max q_e for MB [mg g^{-1}]	E_C/ρ_A [MPa/(g cm^{-3})]	Reference
	CS/GO (2/1) no-GEL aerogel	377	169	31.2	This study
Dye adsorption capacity	PVA/reduced GO (2/1) aerogel	165			Xiao et al., 2017a
	CS/GO (1/7.5) powder	86			Banerjee, Barman, Mukhopadhayay, & Das, 2017
	PVA/reduced GO (2/1) aerogel	250			Xiao et al., 2017b
	CA/GO (2/3) aerogel	62	767		Xiao, Lv, Song & Zheng, 2018
	CS/GO (1/1) aerogel microspheres		180		Yu et al., 2017
	CS/GO (1/1) aerogel		200		Qi, Zhao, Lin & Wu, 2018
	CNF/GO (7/3) aerogel		81		Ma et al., 2016
	Magnetic CS/GO (4/3) powder		180		Fan et al., 2012
Mechanical prop.	CS/reduced GO (1/4) aerogel			15.5	Zhang et al., 2018
	CS/reduced GO (1/5) aerogel			27.9	Li et al., 2018
	PVA/reduced GO (2/1) aerogel			10.7	Xiao et al., 2017b
	CA/GO (2/3) aerogel			25.1	Xiao, Lv, Song & Zheng, 2018

CONCLUSIONS

The goal of the present work was highlighting the relevance of the conditions of preparation of CS-based aerogels in terms of mechanical properties and dye adsorption capacity. Samples were prepared following two procedures, which differ in terms of the order of the sequence of the crosslinking and freeze-drying steps. Apparent density data and porosity measurements showed that the two families of samples share the same overall porosity, but the degree of pore interconnectivity of the samples crosslinked after the freeze-drying step was higher. These samples exhibited better performance in terms of dye adsorption capacity, with an increase of the adsorption ability towards Indigo Carmine of about 45%. Such a notable result was obtained at the price of a reduction of the compressive modulus, which, however, remained high enough for potential applications of the aerogels as adsorbents for wastewater treatment. The addition of GO was found to improve the mechanical strength. The aerogels crosslinked after the freeze-drying step particularly benefited from the reinforcing action of GO, with three times increase of the compressive modulus and negligible propensity to plasticization after repeated loading/unloading cycles. More importantly, all the nanocomposite CS/GO aerogels exhibited broad-spectrum adsorption capacity, being able to retain both anionic (Indigo Carmine, up to 376.8 ± 32.3 mg g^{-1}) and cationic (Methylene Blue, up to 168.6 ± 9.6 mg g^{-1}) dyes owing to the combination of the adsorption features of polymer and nanoparticles. Finally, performing the crosslinking step after the freeze-drying one confirmed to be the better strategy for dye adsorption purposes even for the nanocomposite aerogels.

NOTES

The authors declare no competing financial interest.

ACKNOWLDGMENTS

The work was supported by the Joint Laboratory for “Graphene based Multifunctional Polymer Nanocomposites” funded by CNR (Joint Lab Call 2015–2018), the Key Program for International Science and Technology Innovation Cooperation Between China and Italy Government (2016YFE0104000), and the GRAPE-MAT project “Graphene and perovskite hybrid materials for energy and environment applications”, Progetto Grande Rilevanza Italia-Cina MAECI (2015-2018). The authors also acknowledge A. Aldi and F. Docimo for the technical assistance in the experiments.

APPENDIX A. SUPPLEMENTARY DATA

Supplementary data associated with this article can be found in the online version.

REFERENCES

Argüelles-Monal, W., Goycoolea, F. M., Peniche, C., & Higuera-Ciapara, I. (1998). Rheological study of the chitosan/glutaraldehyde chemical gel system. *Polymer Gels and Networks, 6*, 429-440.

Banerjee, P., Barman, S. R., Mukhopadhayay, A., & Das, P. (2017). Ultrasound assisted mixed azo dye adsorption by chitosan–graphene oxide nanocomposite. *Chemical Engineering Research and Design, 117*, 43-56.

Berger, J., Reist, M., Mayer, J. M., Felt, O., Peppas, N. A., & Gurny, R. (2004). Structure and interactions in covalently and ionically crosslinked chitosan hydrogels for biomedical applications. *European Journal of Pharmaceutics and Biopharmaceutics*, 57, 19-34.

Bhatnagar, A., & Sillanpää, M. (2009). Applications of chitin-and chitosan-derivatives for the detoxification of water and wastewater - a short review. *Advances in Colloid and Interface Science*, *152*, 26-38.

Bhattarai, N., Gunn, J., & Zhang, M. (2010). Chitosan-based hydrogels for controlled, localized drug delivery. *Advanced Drug Delivery Reviews*, 62, 83-99.

Chabot, V., Higgins, D., Yu, A., Xiao, X., Chen, Z., & Zhang, J. (2014). A review of graphene and graphene oxide sponge: material synthesis and applications to energy and the environment. *Energy & Environmental Science*, *7*, 1564-1596.

Chang, X., Chen, D., & Jiao, X. (2008). Chitosan-based aerogels with high adsorption performance. *Journal of Physical Chemistry B*, *112*, 7721-7725.

Chen, Y., Chen, L., Bai, H., & Li, L. (2013). Graphene oxide–chitosan composite hydrogels as broad-spectrum adsorbents for water purification. *Journal of Materials Chemistry A*, *1*, 1992-2001.

Crini, G., & Badot, P. M. (2008). Application of chitosan, a natural aminopolysaccharide, for dye removal from aqueous solutions by adsorption processes using batch studies: a review of recent literature. *Progress in Polymer Science*, *33*, 399-447.

Fan, L., Luo, C., Sun, M., Li, X., Lu, F., & Qiu, H. (2012). Preparation of novel magnetic chitosan/graphene oxide composite as effective adsorbents toward methylene blue. *Bioresource Technology*, *114*, 703-706.

Freundlich, H. M. F. (1906). Over the adsorption in solution. *Journal of Physical Chemistry*, *57*, 1100-1107.

Frindy, S., Primo, A., Ennajih, H., el Kacem Qaiss, A., Bouhfid, R., Lahcini, M., Essassi, E. M., Garcia, H., & El Kadib, A. (2017). Chitosan–graphene oxide films and CO2-dried porous aerogel microspheres: Interfacial interplay and stability. *Carbohydrate Polymers*, *167*, 297-305.

Hummers W. S., & Offeman, R. E. (1958). Preparation of graphitic oxide. *Journal of the American Chemical Society*, *80*, 1339-1339.

Kemp, K. C., Seema, H., Saleh, M., Le, N. H., Mahesh, K., Chandra, V., & Kim, K. S. (2013). Environmental applications using graphene composites: water remediation and gas adsorption. *Nanoscale*, *5*, 3149-3171.

Langmuir I. (1916). The constitution and fundamental properties of solids and liquids. *Journal of the American Chemical Society*, *38*, 2221–2295.

Lavorgna, M., Piscitelli, F., Mangiacapra, P., & Buonocore, G. G. (2010). Study of the combined effect of both clay and glycerol plasticizer on the properties of chitosan films. *Carbohydrate Polymers*, *82*, 291-298.

Li, A., Lin, R., Lin, C., He, B., Zheng, T., Lu, L., & Cao, Y. (2016). An environment-friendly and multi-functional absorbent from chitosan for organic pollutants and heavy metal ion. *Carbohydrate Polymers*, *148*, 272-280.

Li, Z., Song, X., Cui, S., Jiao, Y., & Zhou, C. (2018). Fabrication of macroporous reduced graphene oxide composite aerogels reinforced with chitosan for high bilirubin adsorption. *RSC Advances*, *8*, 8338-8348.

Ma, Z., Liu, D., Zhu, Y., Li, Z., Li, Z., Tian, H., & Liu, H. (2016). Graphene oxide/chitin nanofibril composite foams as column adsorbents for aqueous pollutants. *Carbohydrate Polymers*, *144*, 230-237.

528 Maleki, H. (2016). Recent advances in aerogels for environmental remediation applications: a
529 review. *Chemical Engineering Journal*, *300*, 98-118.
530 Maleki, H., Durães, L., García-González, C. A., del Gaudio, P., Portugal, A., & Mahmoudi, M.
531 (2016). Synthesis and biomedical applications of aerogels: Possibilities and challenges.
532 *Advances in Colloid and Interface Science*, *236*, 1-27.
533 Mi, F. L., Kuan, C. Y., Shyu, S. S., Lee, S. T., & Chang, S. F. (2000). The study of gelation
534 kinetics and chain-relaxation properties of glutaraldehyde-cross-linked chitosan gel and their
535 effects on microspheres preparation and drug release. *Carbohydrate Polymers*, *41*, 389-396.
536 Mikkonen, K. S., Parikka, K., Ghafar, A., & Tenkanen, M. (2013). Prospects of polysaccharide
537 aerogels as modern advanced food materials. *Trends in Food science & Technology*, *34*, 124-
538 136.
539 Monteiro Jr, O. A., & Airoldi, C. (1999). Some studies of crosslinking chitosan–glutaraldehyde
540 interaction in a homogeneous system. *International Journal of Biological Macromolecules*,
541 *26*, 119-128.
542 Nagireddi, S., Katiyar, V., & Uppaluri, R. (2017). Pd (II) adsorption characteristics of
543 glutaraldehyde cross-linked chitosan copolymer resin. *International Journal of Biological*
544 *Macromolecules*, *94*, 72-84.
545 Nieto-Suárez, M., López-Quintela, M. A., & Lazzari, M. (2016). Preparation and
546 characterization of crosslinked chitosan/gelatin scaffolds by ice segregation induced self-
547 assembly. *Carbohydrate Polymers*, *141*, 175-183.
548 Normand, V., Muller, S., Ravey, J. C., & Parker, A. (2000). Gelation kinetics of gelatin: A
549 master curve and network modeling. *Macromolecules*, *33*, 1063-1071.

Olivera, S., Muralidhara, H. B., Venkatesh, K., Guna, V. K., Gopalakrishna, K., & Kumar, Y. (2016). Potential applications of cellulose and chitosan nanoparticles/composites in wastewater treatment: A review. *Carbohydrate Polymers*, *153*, 600-618.

Omidi, S., & Kakanejadifard, A. (2018). Eco-friendly synthesis of graphene–chitosan composite hydrogel as efficient adsorbent for Congo red. *RSC Advances*, *8*, 12179-12189.

Poon, L., Wilson, L. D., & Headley, J. V. (2014). Chitosan-glutaraldehyde copolymers and their sorption properties. *Carbohydrate Polymers*, *109*, 92-101.

Qi, C., Zhao, L., Lin, Y., & Wu, D. (2018). Graphene oxide/chitosan sponge as a novel filtering material for the removal of dye from water. *Journal of Colloid and Interface Science*, *517*, 18-27.

Quignard, F., Valentin, R., & Di Renzo, F. (2008). Aerogel materials from marine polysaccharides. *New Journal of Chemistry*, *32*, 1300-1310.

Roberts, G. A. F., & Taylor, K. E. (1989). Chitosan gels, 3. The formation of gels by reaction of chitosan with glutaraldehyde. *Die Makromolekulare Chemie*, *190*, 951-960.

Sabnis, S., & Block, L. H. (1997). Improved infrared spectroscopic method for the analysis of degree of N-deacetylation of chitosan. *Polymer Bulletin*, *39*, 67-71.

Salzano de Luna, M., Altobelli, R., Gioiella, L., Castaldo, R., Scherillo, G., & Filippone, G. (2017a). Role of polymer network and gelation kinetics on the mechanical properties and adsorption capacity of chitosan hydrogels for dye removal. *Journal of Polymer Science Part B: Polymer Physics*, *55*, 1843-1849.

Salzano de Luna, M., Castaldo, R., Altobelli, R., Gioiella, L., Filippone, G., Gentile, G., & Ambrogi, V. (2017). Chitosan hydrogels embedding hyper-crosslinked polymer particles as reusable broad-spectrum adsorbents for dye removal. *Carbohydrate Polymers*, *177*, 347-354.

Smirnova, I., & Gurikov, P. (2017). Aerogels in chemical engineering: strategies toward tailor-made aerogels. *Annual Review of Chemical and Biomolecular Engineering*, *8*, 307-334.

Tan, H., Wu, J., Lao, L., & Gao, C. (2009). Gelatin/chitosan/hyaluronan scaffold integrated with PLGA microspheres for cartilage tissue engineering. *Acta Biomaterialia*, *5*, 328-337.

Vakili, M., Rafatullah, M., Salamatinia, B., Abdullah, A. Z., Ibrahim, M. H., Tan, K. B., Gholami, Z., & Amouzgar, P. (2014). Application of chitosan and its derivatives as adsorbents for dye removal from water and wastewater: A review. *Carbohydrate Polymers*, *113*, 115-130.

Valentin, R., Molvinger, K., Quignard, F., & Di Renzo, F. (2005). Methods to analyse the texture of alginate aerogel microspheres. *Macromolecular Symposia*, *222*, 93-101.

Wan, W., Zhang, R., Ma, M., & Zhou, Y. (2018). Monolithic aerogel photocatalysts: a review. *Journal of Materials Chemistry A*, *6*, 754-775.

Wang, M., Ma, Y., Sun, Y., Hong, S. Y., Lee, S. K., Yoon, B., Chen, L., Ci, L., Nam, J.-D., Chen, Y., & Suhr, J. (2017). Hierarchical Porous Chitosan Sponges as Robust and Recyclable Adsorbents for Anionic Dye Adsorption. *Scientific Reports*, *7*, 18054.

Winter, H. H., & Chambon, F. (1986). Analysis of linear viscoelasticity of a crosslinking polymer at the gel point. *Journal of Rheology*, *30*, 367-382.

Xiao, J., Lv, W., Song, Y., & Zheng, Q. (2018). Graphene/nanofiber aerogels: Performance regulation towards multiple applications in dye adsorption and oil/water separation. *Chemical Engineering Journal*, *338*, 202-210.

Xiao, J., Lv, W., Xie, Z., Song, Y., & Zheng, Q. (2017a). l-cysteine-reduced graphene oxide/poly (vinyl alcohol) ultralight aerogel as a broad-spectrum adsorbent for anionic and cationic dyes. *Journal of Materials Science*, *52*, 5807-5821.

Xiao, J., Zhang, J., Lv, W., Song, Y., & Zheng, Q. (2017b). Multifunctional graphene/poly (vinyl alcohol) aerogels: In situ hydrothermal preparation and applications in broad-spectrum adsorption for dyes and oils. *Carbon*, *123*, 354-363.

Ye, S., Liu, Y., & Feng, J. (2017). Low-density, mechanical compressible, water-induced self-recoverable graphene aerogels for water treatment. *ACS Applied Materials & Interfaces*, *9*, 22456-22464.

Yu, R., Shi, Y., Yang, D., Liu, Y., Qu, J., & Yu, Z. Z. (2017). Graphene oxide/chitosan aerogel microspheres with honeycomb-cobweb and radially oriented microchannel structures for broad-spectrum and rapid adsorption of water contaminants. *ACS Applied Materials & Interfaces*, *9*, 21809-21819.

Yu, R., Shi, Y., Yang, D., Liu, Y., Qu, J., & Yu, Z. Z. (2017). Graphene oxide/chitosan aerogel microspheres with honeycomb-cobweb and radially oriented microchannel structures for broad-spectrum and rapid adsorption of water contaminants. *ACS Applied Materials & Interfaces*, *9*, 21809-21819.

Zhang, N., Qiu, H., Si, Y., Wang, W., & Gao, J. (2011). Fabrication of highly porous biodegradable monoliths strengthened by graphene oxide and their adsorption of metal ions. *Carbon*, *49*, 827-837.

Zhang, Y., Zhang, L., Zhang, G., & Li, H. J. (2018). Naturally dried graphene-based nanocomposite aerogels with exceptional elasticity and high electrical conductivity. *ACS Applied Materials & Interfaces*, *10*, 21565-21572.

Zhao, S., Malfait, W. J., Guerrero Alburquerque, N., Koebel, M. M., & Nyström, G. (2018). Biopolymer aerogels: Chemistry, properties and applications. An*gewandte Chemie International Edition*, 57, 7580-7608.